

Motion Correction for Kidney Functional Analysis

M G Trad

Department of Electronic Engineering,
University of Surrey, Guildford, GU2 7XH

Magnetic Resonance Imaging (MRI) allows experts to identify any malfunctioning in renal function through glomerular filtration rate (GFR) analysis. However the accuracy of the kidney time-intensity curve is reduced due to the limited resolution of medical imaging systems. Hence the need for motion correction to be applied to the low-resolution image data. To simulate kidney displacement in a free-breathing patient, a movement model is applied to a synthetic kidney created using a data generator. Regions of interest are drawn on the clinical data and underlying tissue characteristics are added to the kidney model. Image registration is performed on the synthetic data and optimum displacement vectors are found. The robustness against noise of two motion correction techniques is assessed.

Introduction

While urine and blood sample tests aim to determine whether both kidneys are functional, imaging tests provide clinicians with separate information about each kidney. Renography is used to localise morphological abnormalities in kidney compartments and detect problems. Figure 1 is a sagittal view of a kidney cross-section.

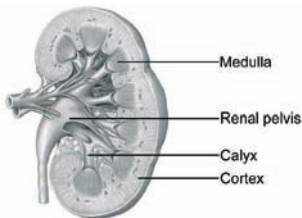


Figure 1. Sagittal cross-section showing the different kidney compartments.

Like any other image acquisition method MRI has its constraints and limits. In the respiratory cycle kidneys are subject to a slight movement. Part of the information in the image acquisition system output is corrupted or lost as a result of motion, leading to biased glomerular filtration rate measurements.

To evaluate renal function a contrast agent (gadolinium) is administered to a patient. Signal intensity changes during agent assimilation, as shown in figure 2.

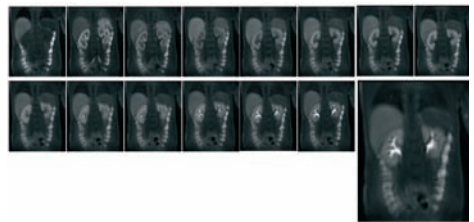


Figure 2. Brightness model showing the variation of contrast agent concentration in kidney compartments.

Images used in the study (figure 3) were acquired using a 1.494 Tesla Siemens Avanto scanner at the Great Ormond Street Hospital, London on 24 May 2006. Slice thickness is 7.5mm, repetition time is 1.63ms, echo time is 0.53ms, bandwidth is 1500Hz/pixel and flip angle is 17°.

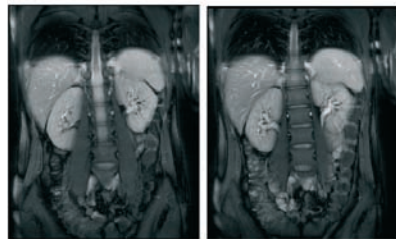


Figure 3. Contraction/dilatation observed on hi-resolution abdominal structures.

Conclusions and discussion

The time-intensity curve of figure 4 is a plot of the average masked data versus the number of volumes. The average masked data is the average of non-zero voxels contained in the window. A data average is computed for every volume.

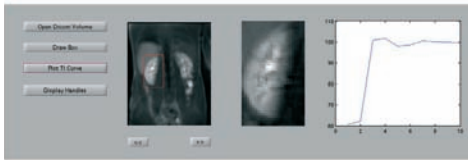


Figure 4: Kidney time-intensity curve. The steep rise in signal intensity corresponds to the migration of the contrast agent in the cortex.

Subtle anatomical or pathological changes occur when images from a patient are taken at slightly different times. In this report, structures are quantified using the sum of absolute differences (SAD) and the sum of squared differences (SSD).

In order to produce high resolution volume templates corresponding to kidney compartments and abdominal structures, 3D geometrical surfaces are drawn and anatomical volumes are labeled. Movement correction can be assessed by the introduction of a movement model that produces ground truth displacement data. At this stage tissue values are allocated to kidney compartments and noise is added to the data. Finally the high resolution data is downsampled into a lower resolution. The downsampling process involves filtering and decimating the high resolution data using the acquisition system characteristic point spread function as specified in figure 5.

Referring to figure 4, three case studies are considered. A kidney brightness model is defined for the early, middle and late phases at volumes

10, 27 and 119 respectively. Those points coincide with the contrast agent injection into the kidney, its migration from the cortex to the pelvical volume and its concentration in the pelvis.

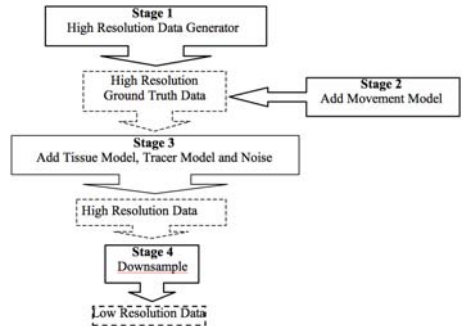


Figure 5. Synthetic data generator flow chart.

Convolving a Gaussian distribution with standard deviation σ_{HR} with the MRI scanner filter's point-spread function results in a blurred and noisy distribution with a different, low-resolution standard deviation σ_{LR} . Test points lie on a straight line of slope 0.044. So for any σ_{LR} ,

The signal-to-noise ratio (SNR) fails to describe how close two tissues are from overlapping in the intensity-frequency plane: two adjacent tissues might have different signal strengths and noise associated to them but still have the same signal-to-noise ratio. The *contrast-to-noise ratio* (CNR) makes the distinction between a number of contrasts in an image and the inherent noise in it possible and is defined as

where $\Delta\mu$ is the difference between the signal intensities of two tissues and σ is the standard deviation of the Gaussian distribution of one of the tissues.

Kidney compartment and background tissues are obtained by manually drawing regions of interests on the clinical data (figure 6).

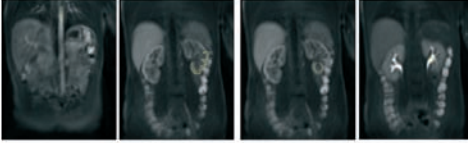


Figure 6. Application of data masks on clinical data. Underlying tissue portions are specified by the yellow regions of interest.

Mean and hi-resolution standard deviation values, used in the tracer model file to quantify the kidney contrast-to-noise ratio at the early, middle and late phase, are gathered in table 1.

Slice	Cortex		Pelvis		Medulla		Aorta		Background	
	μ	σ	μ	σ	μ	σ	μ	σ	μ	σ
8	55	614	29	134	34	86	57	206	35	74
9	69	811	39	151	37	116	72	257	36	82
10	58	523	30	114	38	173	63	261	38	64
11	75	1,100	41	170	33	86	57	275	35	64
12	40	163	29	140	34	67	90	369	34	66
25	149	386	69	636	112	432	179	295	45	114
26	143	409	76	523	99	318	177	386	46	113
27	148	364	71	568	107	364	161	482	47	136
28	141	386	67	432	107	318	193	386	48	114
29	154	386	77	454	119	364	185	273	48	114
117	141	364	397	1,591	163	182	141	204	46	136
118	146	477	346	1,114	170	204	134	136	44	182
119	139	341	405	1,477	163	568	138	477	47	91
120	148	364	370	1,182	161	159	148	182	48	159
121	145	341	409	1,636	165	250	139	136	47	114

Table 1. Values of μ and σ in the early, middle and late phase.

Using the data generator two low-resolution volumes are created. Assuming a purely vertical kidney motion in the y direction, volume0 is centred at (0; 0; 0) and volume1 is centred at (0; -5; 0) in the spatial domain. Assuming a 21-by-21 search window centred at (0;-5) allowing a maximum kidney displacement of ± 10 pixels in the x and y directions, a distortion measure, the sum of

absolute differences, is calculated for all 441 search positions.

$$SAD = \sum_{x_{min}=-10}^{x_{max}=10} \sum_{y_{min}=-15}^{y_{max}=5} |Exp_v1s5 - Th_v1s5|$$

The metric finds the similarity between two images; the greater their similarity the smaller the sum of absolute differences. The smallest distortion measure yields the optimum motion vector.

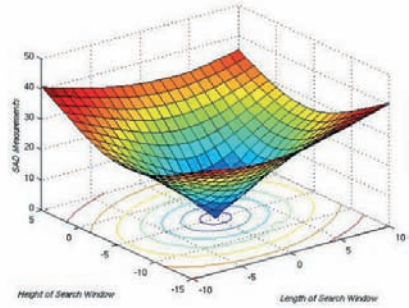


Figure 7. Displacement vector calculation in the absence of noise using SAD. The sum of absolute differences is divided by the size of the search window (21x21).

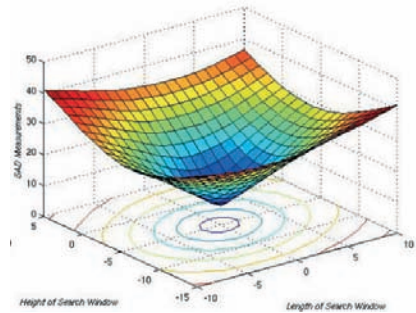


Figure 8. Displacement vector calculation in the absence of noise using SAD. The sum of absolute differences is divided by the size of the kidney box (73x55).

Although both graphs start off with the *same*, *wide*, cone-like shape, however the graph in figure 7 *spirals down* to the answer more rapidly. The distance between the concentric gradient circles decreases swiftly as the true displacement vector is approached (figure 7).

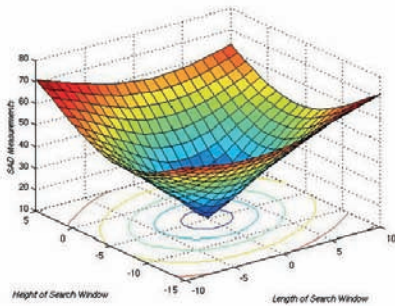


Figure 9. Displacement vector calculation in the presence of noise using SAD.

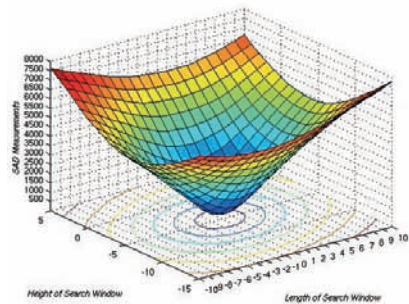


Figure 10. Displacement vector calculation in the presence of noise using SSD.

Although the graph of figure 9 *spirals down* to the answer despite the presence of noise, however it does not predict the true motion vector as accurately as the graph in figure 7. The distance between the concentric gradient circles decreases more swiftly in the absence of noise (figure 7) than in the presence of noise (figure 8).

Although both graphs start off with the *same*, *wide*, cone-like shape, however the graph in figure 9 *spirals down* to the answer more effectively. On the other hand the distance between the concentric gradient circles decreases more swiftly in the graph in figure 10 than the one in figure 9 as the true displacement vector is approached.

Conclusion

Respiratory motion causes a series of translations and rotations of the kidney. However, to simplify the kidney motion model, rotations are not included in the generator movement model file for the sum of absolute difference and the sum of squared difference techniques are limited to a two-dimensional space.

An interesting aspect of the data generator is that non-integer displacement vectors can be specified, thereby testing the accuracy of registration techniques on sub-pixel kidney motion.

As a result of being injected with Gadolinium, a patient's kidney can be characterised by a brightness parameter that is best captured by contrast-to-noise ratios.

Clinical data analysis requires that images be registered accurately. The aim is to move a region of interest in volume 0 by a precalculated displacement vector to its new position in volume 1. The vectors are obtained by correlating both volumes.

The treatment of functional data in the acquisitions yields valuable information on kidney function. In order to assess the model performance on the medical image database, a functional data generator was used to produce a synthetic kidney to which a predefined movement model was applied.

Acknowledgements

The author would like to thank Dr Kevin Wells, Director of the Biomedical Imaging Group at the University of Surrey and project supervisor, for his valuable guidance and advice throughout the project.

References

1. Denis de Senneville B, Ries M, Desbarats P, Moonen C T W and Grenier N Kidney tracking for MR glomerular filtration rate analysis
2. Hill D L G, Batchelor P G, Holden M and Hawkes D J 2001 Medical image registration *Phys. Med. Biol.* 46 1-45
3. Rodriguez Gutierrez D 2006 Synthetic functional data generator
4. Giele E L W 2002 Computer methods for semi-automatic MR renogram determination
5. Giele E L W, de Priester J A, Blom J A, den Boer J A, van Engelshoven J M A and Hasman A 2000 Reduction of noise in medullary renograms from dynamic MR images *J. Magn. Reson. Imaging* 11:149-155
6. Gottesfeld Brown L 1992 A survey of image registration techniques *ACM Computing Surveys* 24 325-376
7. Cox R W and Jesmanowicz A 1999 Real-time 3D image registration for functional MRI *Magn. Reson. Med.* 42 1014-1018
8. Woods R P, Grafton S T, Holmes C J, Cherry S R, Mazziotta J C 1998 Automated image registration: general methods and intrasubject, intramodality validation *J. Comp. Assisted Tomography* 22 39-152